Available online at www.sciencedirect.com

ScienceDirect

MATTER AND RADIATION AT EXTREMES

Matter and Radiation at Extremes 1 (2016) 269–276

www.journals.elsevier.com/matter-and-radiation-at-extremes

Research Article

Thermal equation of state of a natural kyanite up to 8.55 GPa and 1273 K

Qiang He [a,b,c], Xi Liu [a,b,*], Baosheng Li [d], Liwei Deng [e], Wei Liu [d], Liping Wang [f]

[a] Key Laboratory of Orogenic Belts and Crustal Evolution, Ministry of Education of China, Beijing 100871, China
[b] School of Earth and Space Sciences, Peking University, Beijing 100871, China
[c] Institute of Fluid Physics, China Academy of Engineering Physics, Mianyang 621900, China
[d] Mineral Physics Institute, Stony Brook University, Stony Brook, NY 11794-2100, USA
[e] Institute of Geology and Geophysics, Chinese Academy of Sciences, Beijing 100029, China
[f] High Pressure Science and Engineering Center and Department of Physics and Astronomy, University of Nevada, Las Vegas, NV 89154, USA

Received 10 May 2016; revised 12 July 2016; accepted 27 July 2016
Available online 24 August 2016

Abstract

The thermal equation of state of a natural kyanite has been investigated with a DIA-type, cubic-anvil apparatus (SAM85) combined with an energy-dispersive synchrotron X-ray radiation technique up to 8.55 GPa and 1273 K. No phase transition was observed in the studied pressure-temperature (P-T) range. The Le Bail full profile refinement technique was used to derive the unit-cell parameters. By fixing the bulk modulus K_0 as 196 GPa and its pressure derivative K_0' as 4, our P-V (volume)-T data were fitted to the high temperature Birch–Murnaghan equation of state. The obtained parameters for the kyanite are: $V_0 = 294.05(9)$ Å^3, $\alpha = 2.53(11) \times 10^{-5}$ K^{-1} and $(\partial K/\partial T)_P = -0.021(8)$ GPa·K^{-1}. These parameters have been combined with other experimentally-measured thermodynamic data for the relevant phases to calculate the P-T locus of the reaction kyanite = stishovite + corundum. With this thermodynamically constrained phase boundary, previous high-pressure phase equilibrium experimental studies with the multi-anvil press have been evaluated.

PACS codes: 91.67.-y; 91.65.-n; 91.60.Fe; 91.60.Gf

Keywords: Kyanite; X-ray diffraction; Thermal equation of state; High-pressure and high-temperature; Kyanite decomposition; Thermodynamic calculation

1. Introduction

Kyanite (ideally Al_2SiO_5; $P\bar{1}$) is a typical metamorphic mineral, and frequently occurs in metapelites [1], amphibolites [2], and peraluminous eclogites [3]. It participates in many metamorphic reactions which usually involve paragonite, zoisite, lawsonite, pumpellyite, stishovite and so on, thus is very useful in understanding the pressure-temperature (P-T) conditions of these metamorphic rocks. It is also a major phase in subducted sediment and continental crust at the P-T conditions of the upper mantle [4,5]. As an example, anorthite, an important phase in the sediment and continental crust, breaks down to kyanite + quartz + grossular at ~2.5 GPa [6–8]. As another example, orthoclase, another important phase in the sediment and continental crust, breaks down to kyanite + coesite + $K_2Si_4O_9$-wadeite at ~6 GPa [9–11]. In order to fully understand the behavior of kyanite under these geological circumstances, it is necessary to precisely know the thermal equation of state (TEoS) of kyanite.

Volumetric thermal expansion coefficient α and isothermal bulk modulus K_0 at ambient P-T condition are two fundamental parameters for a TEoS. So far the parameter α of kyanite has been investigated in four experimental studies, as summarized in Table 1 [12–15]. We individually re-fitted the

* Corresponding author. School of Earth and Space Sciences, Peking University, Beijing 100871, China. Fax: +86 10 6275 2996.
E-mail address: xi.liu@pku.edu.cn (X. Liu).
Peer review under responsibility of Science and Technology Information Center, China Academy of Engineering Physics.

http://dx.doi.org/10.1016/j.mre.2016.07.003

Table 1
Thermal expansion coefficients of kyanite at ambient *P-T* condition.

α[a] (10^{-5} K^{-1})	Sample	Method	Max. *T* (K)	Data source
2.78(7)	Powder	XRD[b]	1328	[12]
2.51(6)	Single crystal	XRD	1073	[13]
2.48(3)	Powder	ND[c]	1473	[14]
2.47(5)	Powder	XRD	1273	[15]
2.50(3)	–	–	1473	[13–15]

[a] α treated as *T*-independent.
[b] X-ray diffraction.
[c] Neutron diffraction.

volume (*V*)-temperature data in the four studies according to the definition of thermal expansion coefficient ($\alpha = V^{-1}\cdot\partial V/\partial T$). Within the resolution of the data, the derived thermal expansion coefficients seemed temperature-independent. The result constrained by the data from Ref. [12] was slightly different from that constrained by any of the other studies. Consequently, we put the volume-temperature data from all other studies together, and derived a nominally average thermal expansion coefficient for kyanite ($2.50(3) \times 10^{-5}$ K^{-1}; Table 1). The isothermal bulk modulus of kyanite has been investigated both by high pressure experiments and by theoretical simulations [16–23]. As summarized in Ref. [23], the acceptable isothermal bulk modulus and its first pressure derivative of kyanite at ambient temperature are thought to be close to 196(6) GPa and 4.0, respectively.

With the thermal expansion coefficient at ambient pressure and isothermal bulk modulus at ambient temperature, the TEoS of kyanite can be roughly approximated by ignoring the temperature effect on the isothermal bulk modulus. However, the deep Earth is a high-*P* and high-*T* environment, so that it would be desirable to constrain the TEoS of kyanite with experiments under simultaneous high *P* and high *T*. So far, this type of experiment has not been available for kyanite. In this study, we used a cubic-anvil apparatus combined with a synchrotron X-ray radiation technique to conduct compression experiments at simultaneously high *P* and high *T* to constrain the TEoS of kyanite. Further, the experimentally-obtained TEoS was used to thermodynamically calculate the high-*P* breakdown reaction of kyanite (kyanite = stishovite + corundum).

2. Experimental method

The natural kyanite sample used in this study was identical to what was used in Refs. [15,23]. Its chemical composition is $(Al_{1.99}Fe_{0.01})SiO_5$.

The high-pressure and high-temperature experiments were performed using the DIA-type cubic-anvil apparatus (SAM85) installed at the superconducting wiggler beam line X17B2 of the National Synchrotron Light Source, Brookhaven National Laboratory. The details of the experimental setup were similar to those used in Ref. [24]. A specimen sandwich with the NaCl powder sandwiched by the powders of kyanite and CAS (Ca-Al-Si rich phase with the composition $CaAl_4Si_2O_{11}$; to be reported elsewhere) was enclosed in an *h*BN capsule. Amorphous graphite was used as the heating element, and amorphous boron epoxy was used as the pressure medium. The chamber pressure was determined by the TEoS of NaCl [25]. The chamber temperature was measured using a $W_{97}Re_3$-$W_{75}Re_{25}$ thermocouple placed adjacent to the specimen at halfway along the graphite heater, with any high pressure effect on the electromotive force of the thermocouple ignored. The temperature uncertainty should be less than 20 K, according to Ref. [26]. The incident X-ray beam was collimated to 0.2 mm (horizontal) by 0.1 mm (vertical), and the diffraction angle was set at $2\theta = 6.621(2)^\circ$. The X-ray diffraction data from the sample and NaCl pressure standard were collected in an energy dispersive mode using a solid-state Ge detector.

In the *P-V-T* experiments, the sample was initially compressed to a ram load of 64.9 MPa oil pressure and then heated to 1273 K. While the ram load was kept constant, the temperature was reduced with stops at 1073, 873, 673, 473, 298 K, and the X-ray data were collected at each temperature stop. After finishing this heating-cooling cycle, the ram load was decreased to the next target pressure followed by another heating-cooling cycle. In total five heating-cooling cycles were performed, and their exact *P-T* paths were shown in Fig. 1.

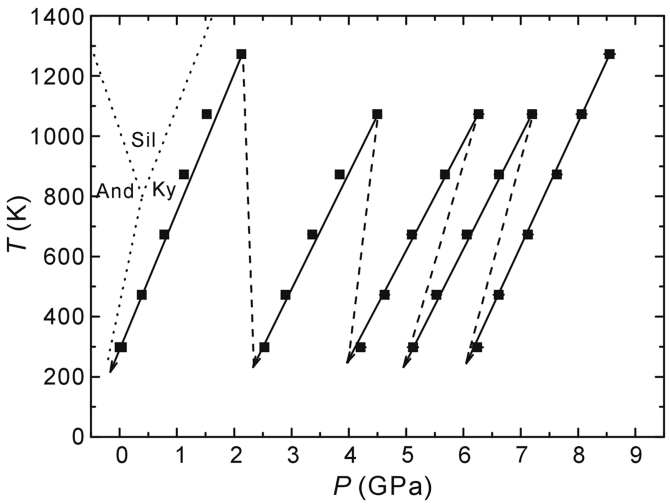

Fig. 1. *P-T* paths of our experiments. The phase relations of andalusite (And)-sillimanite (Sil)-kyanite (Ky) at low pressure are sketched from Hu et al. [27].

3. Result

Using the GSAS soft package [28] and the EXPGUI [29], the XRD data were processed by the Le Bail full profile fit method [30], with the initial structural parameters of kyanite from Ref. [18]. A representative of the fitted XRD patterns for the kyanite sample is shown in Fig. 2. Besides the diffraction peaks of kyanite or NaCl, eight contaminant peaks were constantly observed, and all of them could be attributed to the *h*BN capsule material. On the other hand, no peaks were observed for the amorphous graphite heater and boron epoxy pressure medium. The result from the Le Bail full profile fit always attained high confidence level (for instance, $R_p = \sum|I_o - I_c|/\sum I_o = 0.035$ and reduced $\chi^2 = 3.80$ for the profile shown in Fig. 2, with I_o and I_c as the observed and calculated intensities of the individual peak).

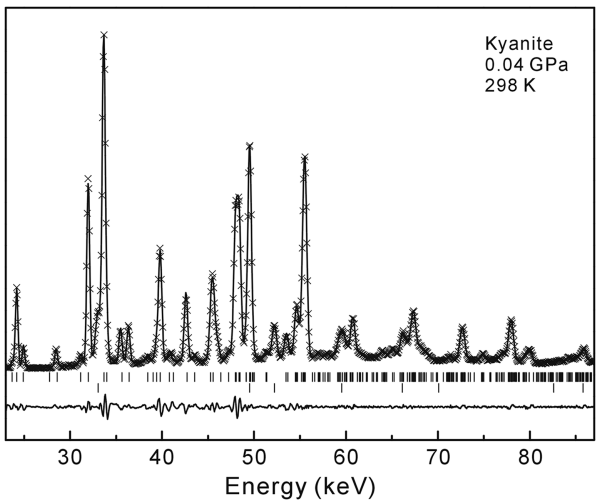

Fig. 2. A representative XRD pattern of kyanite: experimentally-observed (crosses) versus calculated (solid curve) by the GSAS program. The first row of vertical bars represents the XRD peaks of the kyanite sample while the second row the *h*BN capsule material.

The derived unit-cell volumes of the kyanite are listed in Table 2. Our observed unit-cell volume at ambient *P-T* condition, 293.84(3) Å^3, is in good agreement with early reports [12–15,19,23]. In addition, our experimental *P* and *T* covered the *P* range from 0.10 MPa (1 atm) to 8.55 GPa and *T* range from 298 K to 1273 K, and remained in the *P-T* stability field of kyanite [27]. As expected, no phase transition from kyanite to either andalusite or sillimanite was observed in this study (Fig. 1).

The Birch–Murnaghan equation of state (BM-EoS) was employed to fit our data. Its room-*T* form is written as:

$$P = (3/2)K_0\left[(V_0/V)^{7/3} - (V_0/V)^{5/3})\right] \times \left\{1 + 3/4\left(K_0' - 4\right)\left[(V_0/V)^{2/3} - 1\right]\right\}, \quad (1)$$

where K_0 is the isothermal bulk modulus, V_0 the unit-cell volume at room pressure, and K_0' the first pressure derivative of K_0, respectively. Its high-*T* form, which is called TEoS in this study, can be derived by replacing K_0, K_0' and V_0 with their high-*T* equivalents K_T, K_T' and V_T, respectively. These high-*T* forms K_T, K_T' and V_T are defined by the following equations:

$$K_T = K_0 + (\partial K/\partial T)_P(T - T_0), \quad (2)$$

$$K_T' = K_0', \quad (3)$$

and

$$V_T = V_0 \exp\left(\int_{T_0}^{T} \alpha \mathrm{d}T\right), \quad (4)$$

where $(\partial K/\partial T)_P$, T_0, and α are the temperature derivative of the bulk modulus at constant *P*, the reference temperature (298 K), and the volumetric thermal expansion coefficient at atmospheric pressure, respectively. The thermal expansion coefficient α is empirically represented by

$$\alpha(T) = a_0 + a_1 T + a_2 T^{-2}. \quad (5)$$

Our *P-V-T* data have been fitted to this TEoS. During the data-fitting, we fixed the values of K_0 (196 GPa), K_0' (4.0), a_1 (0 K^{-2}) and a_2 (0 K) according to Refs. [15,23]. The derived parameters are $V_0 = 294.05(9)$ Å^3, $(\partial K/\partial T)_P = -0.021(8)$ GPa•K^{-1} and $a_0 = 2.53(11) \times 10^{-5}$ K^{-1}. Apparently, the thermal expansion coefficient determined in this study is temperature-independent ($\alpha = a_0$), and essentially identical to what was found at atmospheric pressure in earlier studies [13–15], as listed in Table 1. On the other hand, our $(\partial K/\partial T)_P$ value is only marginally in the range from −0.0263 to −0.0285 GPa•K^{-1}, thermodynamically estimated using the breakdown reaction kyanite = stishovite + corundum in Ref. [31]. It should be noted that some of the thermodynamic properties such as the isothermal bulk moduli of kyanite and stishovite have been experimentally revised [23,32], with their values significantly modified (160 versus 196 GPa, and 315 versus 296 GPa, respectively), since the thermodynamic analysis was conducted in Ref. [31]. In addition,

Table 2
Volumes of kyanite under different *P-T* conditions.

P_{exp}[a] (GPa)	*T* (K)	*V* (Å^3)	$P_{cal} - P_{exp}$[b] (GPa)	P_{dif}[c] (GPa)
8.55(10)[d]	1273	287.86(3)	−0.26	0.18
8.06(9)	1073	287.65(3)	−0.06	0.18
7.63(8)	873	287.43(3)	0.25	0.21
7.12(9)	673	287.40(4)	0.64	0.25
6.62(9)	473	286.96(4)	0.75	0.36
6.24(10)	298	286.36(3)	0.75	0.52
7.20(8)	1073	288.59(3)	−0.24	0.02
6.62(7)	873	288.37(3)	−0.07	0.12
6.06(8)	673	288.47(3)	0.35	0.24
5.53(9)	473	288.35(3)	0.68	0.35
5.12(9)	298	287.47(3)	0.48	0.45
6.27(8)	1073	290.29(3)	0.05	0.08
5.68(7)	873	289.87(3)	0.06	0.06
5.10(8)	673	289.66(2)	0.26	0.10
4.62(8)	473	289.35(3)	0.51	0.14
4.20(9)	298	288.45(2)	0.30	0.31
4.50(7)	1073	292.97(3)	0.11	0.02
3.84(6)	873	292.36(4)	−0.04	0.09
3.36(8)	673	291.35(3)	−0.29	0.12
2.90(7)	473	290.85(3)	−0.15	0.16
2.53(7)	298	290.17(3)	−0.15	0.27
2.13(3)	1273	297.79(3)	−0.04	0.02
1.52(4)	1073	297.01(2)	−0.23	0.03
1.12(4)	873	296.49(2)	−0.04	0.09
0.78(3)	673	295.75(2)	0.08	0.03
0.39(3)	473	295.16(2)	0.27	0.09
0.04(0)	298	293.84(3)	−0.10	0.11
0.00(0)	298	293.84(3)	−0.14	0.03

[a] Pressure calculated by using the TEoS of NaCl [25], and used in the TEoS fit for kyanite.
[b] Difference between the pressures calculated by using the TEoS of kyanite obtained in this study (P_{cal}) and by using the TEoS of NaCl (P_{exp}).
[c] P_{dif} is the differential stress in the NaCl pressure marker calculated as the difference in the lattice strains of the 222 peak and 400 peak.
[d] Numbers in the parenthesis represent one standard deviation in the right-most digit.

the estimated value of the standard entropy of stishovite in Ref. [31], ranging from 24.62 to 26.25 J•mol^{-1}•K^{-1}, was only in marginal agreement with the newly experimental measurements as well (24.0 J•mol^{-1}•K^{-1} from Ref. [33]; 24.94 J•mol^{-1}•K^{-1} from Ref. [34]).

The experimentally-measured *P-V-T* data are plotted in Fig. 3. All experimental data at 1273, 1073 and 873 K fall close to the TEoS curves at corresponding temperatures. In contrast, the experimental data at 673, 473 and 298 K exhibit different behavior: the data at pressures lower than ~4 GPa agree well with the TEoS curves whereas those at pressures higher than ~4 GPa show relatively large deviation (See Table 2 for the difference between the pressures calculated by using our TEoS of kyanite and by using the TEoS of NaCl). This relatively large deviation at these low *T* and high *P* conditions, ranging from 0.26 to 0.75 GPa, can be explained by differential stress in the kyanite sample.

We can gain some hints on the differential stress in the kyanite sample by calculating the differential stress experienced by the NaCl pressure marker used in our experiments. The differential stress in the NaCl pressure marker was calculated as the difference in the lattice strains of the 222 peak and 400 peak [35]. The results are listed in Table 2 and plotted in Fig. 4. Clearly, the differential stress was positively correlated to *P* increase, but negatively correlated to *T* increase. The largest differential stress, 0.52 GPa, occurred at 6.25 GPa and 298 K. Since the bulk modulus of kyanite (196(6) GPa; Ref. [23]) is much larger than that of NaCl (30.2(3) GPa; fitted from Ref. [25]), since kyanite has a more pronounced elastic anisotropy than NaCl [18,35], and since our kyanite sample was placed farther away from the geometric center of the experimental cell than the NaCl pressure marker, a larger differential stress in our kyanite sample should be expected.

With the deviation of the *P-V-T* data from the TEoS at relatively low *T*-high *P* conditions explained by the differential stress in the kyanite sample, we are confident in the quality of our TEoS. The excellent agreement of the thermal expansion coefficients independently determined by the current data at simultaneous high *P-T* conditions and by the data at room *P* [13–15] is one good indicator. The *P-V* data of kyanite at $P < 10$ GPa from Ref. [23], being obtained under hydrostatic condition with a diamond-anvil cell and closely falling on our TEoS curve at ambient *T*, suggests that the influence on the TEoS fit of kyanite of the low-*T* and high-*P* data with large differential stress has been successfully removed, and a high quality of our TEoS has been secured.

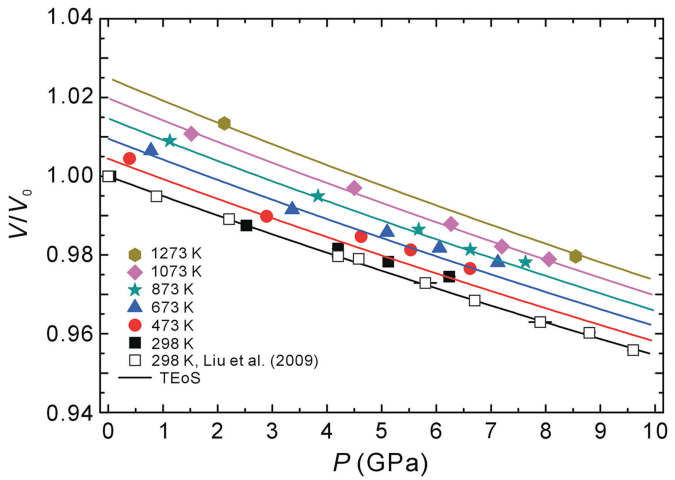

Fig. 3. High-*T* Birch–Murnaghan equation of state of kyanite, drawn as curves. For comparison, the data at $P < 10$ GPa obtained under hydrostatic condition with a diamond-anvil cell [23] are also shown.

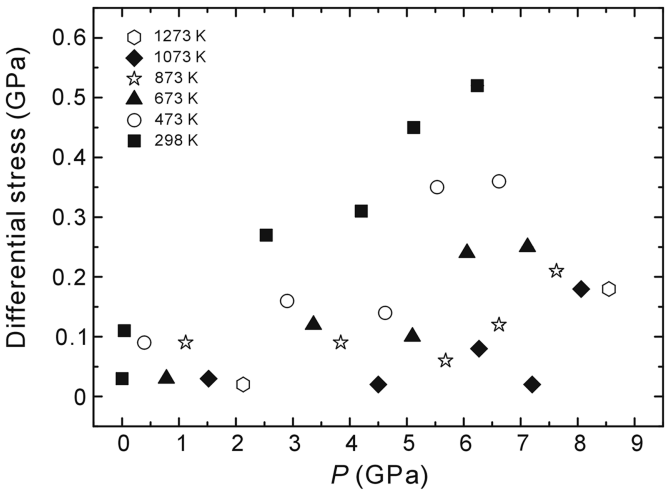

Fig. 4. Differential stress in the NaCl pressure marker.

4. Discussion

Kyanite decomposes into stishovite and corundum at high pressure. This reaction has been experimentally and thermodynamically investigated by several studies [15,31,34,36–39]. Liu [36] performed diamond-anvil cell experiments which were subject to large uncertainties in the *P* and *T* measurements, and his result is thus distinctly different from all other studies. Schmidt et al. [31] and Liu et al. [38] conducted forward and reversal multi-anvil experiments by using conventional quench method, and these two studies were in good agreement within experimental uncertainties (Fig. 5). Irifune et al. [15] and Ono [37] also carried out multi-anvil experiments, and reported very similar *P-T* loci for the kyanite breakdown reaction, which were lower by 1–2 GPa than those constrained by Schmidt et al. [31] and Liu et al. [38]. Recently Ono et al. [39] made in situ observation of this reaction by using a multi-anvil press coupled with synchrotron X-ray radiation, and their result was generally much compatible with those reported by Irifune et al. [15] and Ono [37]. Therefore, all the experimental studies conducted with the multi-anvil press fell into two groups, and the *P* difference between these two groups is about 1–2 GPa in the *T* interval of 1000–1800 K. In addition, Yong et al. [34] thermodynamically investigated this reaction, and their calculated *P-T* locus was close to the results of Irifune et al. [15], Ono [37] and Ono et al. [39].

With the determination of the TEoS of kyanite in this study, all thermodynamic data required to calculate the breakdown reaction of kyanite to stishovite and corundum have been

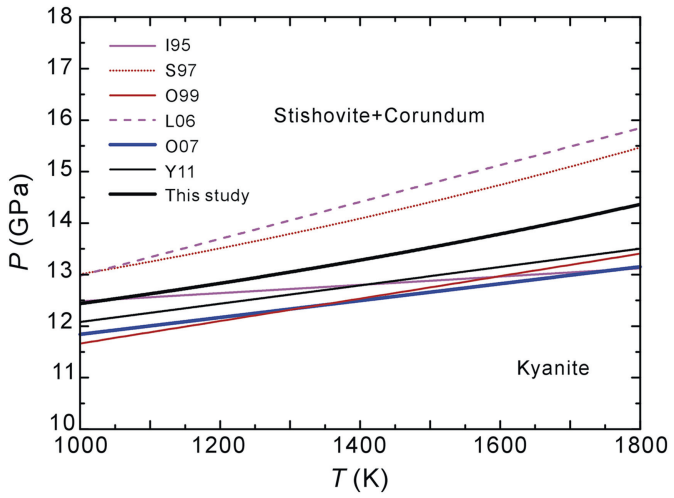

Fig. 5. Phase boundary between kyanite and stishovite + corundum. I95, Ref. [15]; S97, Ref. [31]; O99, Ref. [37]; L06, Ref. [38]; O07, Ref. [39]; Y11, Ref. [34]. The equations for the *P*-*T* locus are *P* (GPa) = $11.7 + 8 \times 10^{-4} \times T$ (K) [15], $P = 10.2 + 1.6 \times 10^{-3} \times T$ (K) [38], $P \approx 9.3 + 3.5 \times 10^{-3} \times T$ (K) [31], and $P = 11.3 + 3.8 \times 10^{-4} \times T + 7.5 \times 10^{-7} \times T^2$ (K) (alternatively $P \approx 10.6 + 1.95 \times 10^{-3} \times T$ (K)); this study.

experimentally measured (Table 3). Consequently, we have thermodynamically calculated this reaction by using the following equations:

$$\Delta_r G_{P,T} = \Delta_r H_T^0 - T\Delta_r S_T^0 + \int_1^P \Delta_r V_T(P)\mathrm{d}P = 0, \quad (6)$$

$$\Delta_r H_T^0 = \Delta_r H_{298}^0 + \int_{298}^T \Delta_r C_p \mathrm{d}T = -\Delta_r H_{d-s}^0 + \int_{298}^T \Delta_r C_p \mathrm{d}T, \quad (7)$$

$$\Delta_r S_T^0 = \Delta_r S_{298}^0 + \int_{298}^T \frac{\Delta_r C_p}{T}\mathrm{d}T, \quad (8)$$

$$\int_1^P \Delta_r V_T(P)\mathrm{d}P = \Delta_r \left[V_{T,P}P - V_T - \int_{V_T}^{V_{T,P}} P(V)\mathrm{d}V \right], \quad (9)$$

and

$$\int_{V_T}^{V_{T,P}} P(V)\mathrm{d}V = \frac{9}{16}K_T V_T \left\{ \left(4 - K_T'\right)\left[\left(\frac{V_T}{V_{T,P}}\right)^2 - 1\right] + \left(3K_T' - 14\right)\left[\left(\frac{V_T}{V_{T,P}}\right)^{4/3} - 1\right] + \left(16 - 3K_T'\right)\left[\left(\frac{V_T}{V_{T,P}}\right)^{2/3} - 1\right]\right\}, \quad (10)$$

where $G_{T,P}$ is the Gibbs free energy at specific P and T, $V_{T,P}$ the molar volume at specific P and T, H_T^0 the enthalpy at high T, H_{d-s}^0 the enthalpy measured with a drop-solution method, C_p the heat capacity, S_T^0 the entropy at high T, and S_{298}^0 the entropy at 298 K. The prefix Δ_r represents the change of the relevant property along the phase boundary.

Our calculated *P*-*T* locus is shown in Fig. 5. Although our calculation has been carried out to 1800 K, we believe that only the *P*-*T* locus below 1300 K or so is of high accuracy because most thermo-elastic parameters such as $(\partial K/\partial T)_P$ and α were usually measured in T ranges from room temperature up to ~1300 K only.

Compared to the thermodynamic calculation result from Yong et al. [34], our result is about 0.5 GPa higher at temperatures around 1300 K (Fig. 5). It should be noted that in our calculation all required thermodynamic data were available, so that the calculation could be fulfilled. In Yong et al. [34], however, they neglected all the $(\partial K/\partial T)_P$ values for the relevant phases because this parameter was not available for kyanite at that time.

Compared to the experimental results determined with the multi-anvil press, our calculated boundary is about 0.5–1 GPa higher than that of Irifune et al. [15], Ono [37] and Ono et al. [39], but about 0.5–1 GPa lower than that of Schmidt et al. [31] and Liu et al. [38]; in other words, our calculated *P*-*T* locus for the breakdown reaction of kyanite to stishovite and corundum lies in between those two groups of experimental results (Fig. 5). Considering the current thermodynamic calculation result, we tend to believe that the small difference of ~1 GPa among the

Table 3
Thermodynamic properties used in the thermodynamic calculation.

Phase	S_{298}^0 (J·mol^{-1}·K^{-1})	ΔH_{d-s}^0 (kJ·mol^{-1})	$C_P = A + BT^{-0.5} + CT^{-2} + DT^{-3}$ (J·mol^{-1}·K^{-1})				V_{298}^0 (cm^3·mol^{-1})	$\alpha = a_0 + a_1T + a_2T^{-2}$ (K^{-1})			K_0 (GPa)	K_0'	$\partial K/\partial T$ (GPa·K^{-1})
			$A(10)$	$B(10^2)$	$C(10^6)$	$D(10^7)$		$a_0(10^{-5})$	$a_1(10^{-8})$	$a_2(10^{-1})$			
Ky	82.8[a]	155.14[b]	24.5	−13.0	−7.08	83.2[a]	44.22[c]	2.53	0	0[c]	196[d]	4[d]	−0.021[c]
Sti	24.94[e]	3.04[f]	8.73	−4.14	−2.74	22.1[g]	14.02[h]	1.26	1.29	0[h]	296[h]	4.2[h]	−0.046[h]
Cor	50.9[a]	106.67[i]	16.1	−10.9	−1.42	−7.65[a]	25.59[j]	2.6	0.181	−6.7[j]	258[j]	4.88[j]	−0.020[j]

[a] Calculated from Ref. [40].
[b] Ref. [41].
[c] This work.
[d] Ref. [23].
[e] Ref. [34].
[f] Ref. [42].
[g] Ref. [33].
[h] Ref. [32].
[i] Ref. [43].
[j] Ref. [44].

studies using the quench experimental method at relatively low temperatures could be attributed to the uncertainty in the *P* measurements in the different laboratories, as suggested by Ono et al. [39]. On the other hand, the ~2 GPa difference at relatively high temperatures seems too large, and was caused not only by the difference in the interlaboratory *P* calibrations, but also by the complicated mechanical behavior of the experimental cells used in the multi-anvil press [45]. Additionally, water might have affected the experimental results in Irifune et al. [15] and Ono [37], as pointed out by Liu et al. [38].

Ono et al. [39] conducted ten in situ runs to investigate the decomposition of kyanite in a multi-anvil press coupled with synchrotron X-ray radiation, so that their experiments should be very accurate in the *P* measurements. Their result, however, is surprisingly different to our thermodynamic calculation (Fig. 5). It is believed that, with the energy-dispersive XRD data in Ono et al. [39], the identification of the constituent phases was very complicated and questionable. Kyanite has the lowest symmetry, many XRD peaks and large unit-cell parameters, so that the resolution of its energy-dispersive XRD data is expected to be low. In addition, the XRD profiles reported in Ono et al. [39] were severely affected by the swarming and extremely strong XRD peaks and fluorescence lines of platinum (pressure marker) and rhenium (capsule material).

The *P-T* paths of the ten runs in Ono et al. [39] are summarized in Fig. 6. As evident in Fig. 6, the *P-T* path of Run 1 remained in the stability field of stishovite + corundum whereas the *P-T* paths of Run 3, Run 4, Run 5, Run 6, Run 7, Run 8 and Run 10 stayed in the stability field of kyanite, so that all these runs did not contribute significantly to the determination of the phase boundary.

Run 2 crossed the phase boundary from the stability field of stishovite + corundum to that of kyanite (Fig. 6), as claimed

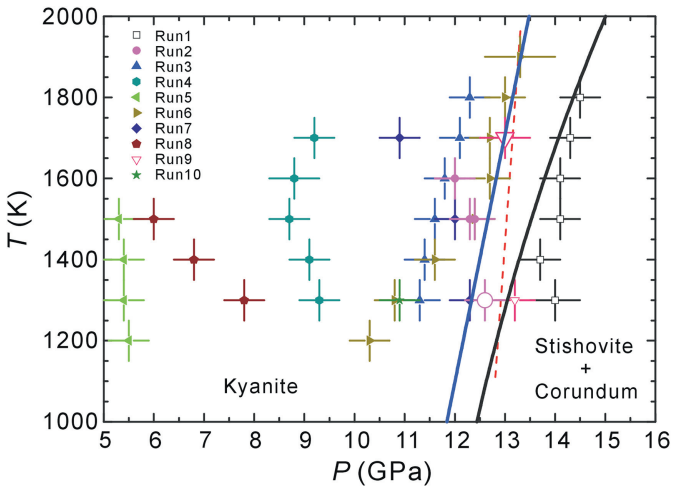

Fig. 6. Comparison of the phase boundary between kyanite and stishovite + corundum determined by Ono et al. [39] and this study. The thick blue curve is taken from Ono et al. [39] while the thick black curve is from this study. The small empty symbols represent the phase assemblage corundum + stishovite whereas the small solid ones represent the phase assemblage kyanite. The two large empty symbols for 2-1 and 9-2 are critical in determining the phase boundary, and have different interpretations: stishovite + corundum [39] versus kyanite (this study).

by Ono et al. [39]. But by comparing the XRD patterns (2-1, 2-2 and 2-3 at 1300 K, 1500 K and 1500 K, respectively; for the information about the labels of the XRD patterns and the *P-T* conditions, see Table 1 in Ref. [39]) of Run 2 shown in their Fig. 3b–d, respectively, we found that the peaks of kyanite labeled as K2-11, K-2-11, K012, K030, K131 and K-331 occurring in the XRD patterns 2-2 (their Fig. 3c) and 2-3 (their Fig. 3d) can also be positively identified in the XRD pattern 2-1 (their Fig. 3b). Since the starting material used in Ono et al. [39] was a mechanical mixture of quartz and corundum, this means that all these XRD patterns were taken from the stability field of kyanite, and Run 2 did not cross the phase boundary at all. Anyhow, the kyanite peaks in the XRD pattern 2-1 were extremely weak. This phenomenon, however, could be readily explained by a potentially slow formation rate of kyanite from the starting material of quartz + corundum at the low *T* of 1300 K, a possible close location of the *P-T* condition to the phase boundary which should be expected to slow down further the formation rate of kyanite, and/or a very short heating duration in the in situ experiments which should have resulted in formation of little kyanite. Using the conventional quench method, Ono et al. [39] conducted two additional experiments with long experimental durations (30 and 90 min, respectively) at the *P-T* conditions (~12.5 GPa and 1350 K, and ~12.4 GPa and 1400 K, respectively) nearly equivalent to those for collecting the XRD pattern 2-1 (~12.6 GPa and 1300 K). Both experiments demonstrated the formation of kyanite, which thus strengthens further our interpretation about the identity of kyanite in the XRD profile 2-1 (12.6 GPa and 1300 K, as represented by the large empty circle in Fig. 6).

Another key XRD pattern to the determination of the phase boundary, 9-2 (as represented by the large empty triangle in Fig. 6), was not shown in Ono et al. [39]. According to Ono et al. [39], this XRD profile demonstrated the coexistence of stishovite and corundum. Due to the factors as discussed in the case of the XRD pattern 2-1, any weak XRD peaks of a small amount of kyanite would have been missed out. Two facts support our speculation. First, if we draw the phase boundary from the middle point between the *P-T* conditions for the XRD profiles 2-1 (12.6 GPa and 1300 K; stability field of kyanite, as discussed above) and 9-1 (13.2 GPa and 1300 K) to the point of the XRD profile 6-8 (13.3 GPa and 1900 K), as shown by the thin broken red line in Fig. 6, the *P-T* condition of the XRD profile 9-2 clearly falls in the stability field of kyanite. Comparing the *P-T* conditions of the XRD profiles of 6-6 (12.7 GPa and 1700 K) and 9-2 (13 GPa and 1700 K), a pressure difference of 0.3 GPa would usually be insufficient to generate a clear-cut experimental result, with the phase assemblage of kyanite in the former while the phase assemblage of stishovite + corundum in the latter for the present case, especially when the heating durations in the in situ experiments were so short.

In summary, our thermodynamically calculated phase boundary agrees with most experimental data from Ono et al. [39], with the only exceptions of the XRD profiles 2-1 and 9-2 (Fig. 6; large empty circle and large empty triangle, respectively). With the detailed discussion in the previous paragraph, we believe that our new determination of the phase boundary

between kyanite and stishovite + corundum has high accuracy. Our thermodynamically calculated phase boundary, closer to the data points demonstrating the phase assemblage stishovite + corundum, is fully compatible with the fact that the experiments in Ono et al. [39] were synthetic experiments with the starting material of stishovite (quickly transferred from quartz) + corundum. In contrast, the phase boundary drawn by Ono et al. [39] seems unusually close to the data points demonstrating the phase assemblage kyanite, considering a potentially significant over-stepping of the phase boundary required by the slow formation rate of kyanite from stishovite (quartz) + corundum, which was experimentally demonstrated to be much slower than the breakdown rate of kyanite to stishovite + corundum [15]. The very short heating durations in the in situ experiments conducted by Ono et al. [39] further undermine the plausibility of their phase boundary.

5. Implication

Kyanite is a key metamorphic mineral, and plays an important role in a large number of metamorphic reactions. For example, the latest internally consistent thermodynamic dataset for phases of petrological interest derived by Holland and Powell [46] was calibrated by using 56 kyanite-involving phase equilibria, in addition to other phase equilibria. However, the values of the properties α, K_0, and $(\partial K/\partial T)_P$ of kyanite were set in the dataset as 1.92×10^{-5} K^{-1}, 160.1 GPa and 0 GPa•K^{-1}, which are rather different to what we have found in this study: $\alpha = 2.53(11) \times 10^{-5}$ K^{-1}, $K_0 = 196(6)$ GPa and $(\partial K/\partial T)_P = -0.021(8)$ GPa•K^{-1}. How these differences can affect the application of this internally consistent thermodynamic dataset is presently unclear, but the preceding discussion about the kyanite breakdown reaction (kyanite = corundum + stishovite) clearly suggests that a careful evaluation is necessary.

Acknowledgements

The in situ X-ray diffraction experiments were carried out at the National Synchrotron Light Source (NSLS), which is supported by the U.S. Department of Energy, Division of Materials Sciences and Division of Chemical Sciences under Contract No. DE-AC02-76CH00016. The operation of X-17B2 is supported by COMPRES, the Consortium for Materials Properties Research in Earth Sciences. This work is financially supported by the Natural Science Foundation of China (Grant No. 41273072) and by the Strategic Priority Research Program (B) of the Chinese Academy of Sciences (XDB18030602).

References

[1] H.M. Lang, Quantitative interpretation of within-outcrop variation in metamorphic assemblage in staurolite-kyanite-grade metapelites, Baltimore, Maryland, Can. Mineral. 29 (1991) 655–671.
[2] R.M. Kuyumjian, Kyanite-staurolite ortho-amphibolite from the Chapada region, Goiás, central Brazil, Mineral. Mag. 62 (1998) 501–507.
[3] M. Vrabec, M. Janák, N. Froitzheim, J.C.M. De Hoog, Phase relations during peak metamorphism and decompression of the UHP kyanite eclogites, Pohorje Mountains (Eastern Alps, Slovenia), Lithos 144–145 (2012) 40–55.
[4] T. Irifune, A.E. Ringwood, W.O. Hibberson, Subduction of continental crust and terrigenous and pelagic sediments: an experimental study, Earth Planet. Sci. Lett. 126 (1994) 351–368.
[5] S. Ono, Stability limits of hydrous minerals in sediment and mid-ocean ridge basalt compositions: implications for water transport in subduction zones, J. Geophys. Res. 103 (1998) 18253–18267.
[6] J.R. Goldsmith, The melting and breakdown reactions of anorthite at high pressures and temperatures, Am. Mineral. 65 (1980) 272–284.
[7] L. Gautron, S. Kesson, W. Hibberson, Phase relations for $CaAl_2S_2O_8$ (anorthite composition) in the system CaO-Al_2O_3-SiO_2 at 14 GPa, Phys. Earth Planet. Inter. 97 (1996) 71–81.
[8] X. Liu, H. Ohfuji, N. Nishiyama, Q. He, T. Sanehira, et al., High-*P* behavior of anorthite composition and some phase relations of the CaO-Al_2O_3-SiO_2 system to the lower mantle of the Earth, and their geophysical implications, J. Geophys. Res. 117 (2012) B09205.
[9] N. Kinomura, S. Kume, M. Koizumi, Synthesis of $K_2SiSi_3O_9$ with silicon in 4- and 6-coordination, Mineral. Mag. 40 (1975) 401–404.
[10] S. Urakawa, T. Kondo, N. Igawa, O. Shimomura, H. Ohno, Synchrotron radiation study on the high-pressure and high-temperature phase relations of $KAlSi_3O_8$, Phys. Chem. Miner. 21 (1994) 387–391.
[11] L. Chang, Z. Chen, X. Liu, H. Wang, Expansivity and compressibility of wadeite-type $K_2Si_4O_9$ determined by in situ high *T*/*P* experiments, and their implication, Phys. Chem. Miner. 40 (2013) 29–40.
[12] B.J. Skinner, S.P. Clark, D.E. Appleman, Molar volumes and thermal expansions of andalusite, kyanite, and sillimanite, Am. J. Sci. 259 (1961) 651–668.
[13] J.K. Winter, S. Ghose, Thermal expansion and high-temperature crystal chemistry of the Al_2SiO_5 polymorphs, Am. Mineral. 64 (1979) 573–586.
[14] G.D. Gatta, F. Nestola, J.M. Walter, On the thermo-elastic behaviour of kyanite: a neutron powder diffraction study up to 1200 °C, Mineral. Mag. 70 (2006) 309–317.
[15] X. Liu, Q. He, H. Wang, M.E. Fleet, X. Hu, Thermal expansion of kyanite at ambient pressure: An X-ray powder diffraction study up to 1000 °C, Geosci. Front. 1 (2010) 91–97.
[16] T. Irifune, K. Kuroda, T. Minagawa, Experimental study of the decomposition of kyanite at high pressure and high temperature, in: T. Yukutake (Ed.), The Earth's Central Part: Its Structure and Dynamics, Terra Scientific Publishing Company, Tokyo, 1995, pp. 35–44.
[17] M. Matsui, Molecular dynamics study of the structures and bulk moduli of crystals in the system CaO-MgO-Al_2O_3-SiO_2, Phys. Chem. Miner. 23 (1996) 345–353.
[18] P. Comodi, P.F. Zanazzi, S. Poli, M.W. Schmidt, High-pressure behavior of kyanite: Compressibility and structural deformations, Am. Mineral. 82 (1997) 452–459.
[19] H. Yang, R.T. Downs, L.W. Finger, Compressibility and crystal structure of kyanite, Al_2SiO_5, at high pressure, Am. Mineral. 82 (1997) 467–474.
[20] A.R. Oganov, J.P. Brodholt, High-pressure phases in the Al_2SiO_5 system and the problem of aluminous phase in the Earth's lower mantle: ab initio calculations, Phys. Chem. Miner. 27 (2000) 430–439.
[21] B. Winkler, M. Hytha, M. Warren, V. Milman, J. Gale, J. Schreuer, Calculation of the elastic constants of the Al_2SiO_5 polymorphs andalusite, sillimanite and kyanite, Z. Krist. 216 (2001) 67–70.
[22] A. Friedrich, M. Kunz, B. Winkler, T. Le Bihan, High-pressure behavior of sillimanite and kyanite: Compressibility, decomposition and indications of a new high-pressure phase, Z. Krist. 219 (2004) 324–329.
[23] X. Liu, S.R. Shieh, M.E. Fleet, L. Zhang, Compressibility of a natural kyanite to 17.5 GPa, Prog. Nat. Sci. 19 (2009) 1281–1286.
[24] B. Li, J. Kung, R.C. Liebermann, Modern techniques in measuring elasticity of Earth materials at high pressure and high temperature using ultrasonic interferometry in conjunction with synchrotron X-radiation in multi-anvil apparatus, Phys. Earth Planet. Inter. 143–144 (2004) 559–574.
[25] D.L. Decker, High-pressure equation of state for NaCl, KCl, and CsCl, J. Appl. Phys. 42 (1971) 3239–3244.

[26] Y.B. Wang, D.J. Weidner, Y. Meng, Advances in equation-of-state measurements in SAM-85, in: M.H. Manghnani, T. Yagi (Eds.), Properties of Earth and Planetary Materials at High Pressure and Temperature, American Geophysical Union, Washington D. C., 1998, pp. 365−372.
[27] X. Hu, X. Liu, Q. He, H. Wang, S. Qin, et al., Thermal expansion of andalusite and sillimanite at ambient pressure: A powder X-ray diffraction study up to 1000 °C, Mineral. Mag. 75 (2011) 363−374.
[28] A.C. Larson, R.B. Von Dreele, General Structure Analysis System (GSAS), Los Alamos National Report LAUR, 2004.
[29] B.H. Toby, EXPGUI, a graphical user interface for GSAS, J. Appl. Crystallogr. 34 (2001) 210−213.
[30] A. Le Bail, Whole powder pattern decomposition methods and applications: A retrospection, Powder Diffr. 20 (2005) 316−326.
[31] M.W. Schmidt, S. Poli, P. Comodi, P.F. Zanazzi, High-pressure behavior of kyanite: Decomposition of kyanite into stishovite and corundum, Am. Mineral. 82 (1997) 460−466.
[32] Y. Nishihara, K. Nakayama, E. Takahashi, T. Iguchi, K. Funakoshi, *P-V-T* equation of state of stishovite to the mantle transition zone conditions, Phys. Chem. Miner. 31 (2005) 660−670.
[33] M. Akaogi, M. Oohata, H. Kojitani, H. Kawaji, Thermodynamic properties of stishovite by low-temperature heat capacity measurements and the coesite-stishovite transition boundary, Am. Mineral. 96 (2011) 1325−1330.
[34] W. Yong, E. Dachs, A. Benisek, Heat capacity, entropy and phase equilibria of stishovite, Phys. Chem. Miner. 39 (2011) 153−162.
[35] N. Funamori, T. Yagi, T. Uchida, Deviatoric stress measurement under uniaxial compression by a powder X-ray diffraction method, J. Appl. Phys. 75 (1994) 4327−4331.
[36] L. Liu, Disproportionation of kyanite to corundum plus stishovite at high pressure and temperature, Earth Planet. Sci. Lett. 24 (1974) 224−228.
[37] S. Ono, High temperature stability limit of phase egg, $AlSiO_3(OH)$, Contrib. Mineral. Petrol. 137 (1999) 83−89.
[38] X. Liu, N. Nishiyama, T. Sanehira, T. Inoue, Y. Higo, et al., Decomposition of kyanite and solubility of Al_2O_3 in stishovite at high pressure and high temperature conditions, Phys. Chem. Miner. 33 (2006) 711−721.
[39] S. Ono, Y. Nakajima, K. Funakoshi, In situ observation of the decomposition of kyanite at high pressures and high temperatures, Am. Mineral. 92 (2007) 1624−1629.
[40] R.A. Robie, B.S. Hemingway, Thermodynamic properties of minerals and related substances at 298.15 and 1 Bar (10^5 Pascals) pressure and at higher temperatures, U.S. Geol. Surv. Bull. 2131 (1995).
[41] M. Akaogi, N. Kamii, A. Kishi, H. Kojitani, Calorimetric study on high-pressure transitions in $KAlSi_3O_8$, Phys. Chem. Miner. 31 (2004) 85−91.
[42] M. Akaogi, H. Yusa, K. Shiraishi, T. Suzuki, Thermodynamic properites of α-quartz, coesite, and stishovite and equilibrium phase relations at high pressures and high temperatures, J. Geophys. Res. 100 (1995) 22337−22347.
[43] H. Kojitani, Y. Wakabayashi, Y. Tejima, C. Kato, M. Haraguchi, et al., High-pressure phase relations in $Ca_2AlSiO_{5.5}$ and energetics of perovskite-related compounds with oxygen defects in the $Ca_2Si_2O_6$−$Ca_2Al_2O_5$ join, Phys. Earth Planet. Inter. 173 (2009) 349−353.
[44] L.S. Dubrovinsky, S.K. Saxena, P. Lazor, High-pressure and high-temperature in situ X-ray diffraction study of iron and corundum to 68 GPa using an internally heated diamond anvil cell, Phys. Chem. Miner. 25 (1998) 434−441.
[45] Y. Fei, C.M. Bertka, Phase transitions in the Earth's mantle and mantle mineralogy, in: Y. Fei, C.M. Bertka, B.O. Mysen (Eds.), Mantle Petrology: Field Observations and High Pressure Experimentation: a Tribute to Francis R. (Joe) Boyd, The Geochemical Society, Houston, 1999, pp. 189−207.
[46] T.J.B. Holland, R. Powell, An imporved and extended internally consistent thermodynamic dataset for phases of petrological interest, involving a new equation of state for solids, J. Metamorph. Geol. 29 (2011) 333−383.